Summer 2020

Phase-Locked Loop Control In Low-Inertia Grid-Connected Voltage-Source Converters

Ifechukwude Gideon Odogwu

PHASE-LOCKED LOOP CONTROL IN LOW-INERTIA GRID-CONNECTED VOLTAGE-SOURCE CONVERTERS

by

IFECHUKWUDE ODOGWU

(Under the Direction of Masoud Davari)

ABSTRACT

As the integration of renewable energy on the grid increases, the number of voltage-source converters (VSC) installed also does. VSC controls both switch turn-on and turn-off, allowing a dc voltage source to be switched between phases. For the converter to accurately synchronize with the grid, a phase-locked loop (PLL) is used for the frequency measurements of the grid. However, the implementation of PLL with measurement delay introduces harmonics, noise, high frequency, and voltage oscillation to the system due to its dynamics. The dynamics introduced to the grid can be ignored under stiff grid conditions, but power from renewable sources decreases the grid inertia creating a weak-grid condition. Older grids accommodate this by using generators that compensate for the rate of change of frequency (RoCoF). Modern grids have less generator to accommodate the RoCoF, so there is a desideratum to implore a robust controller that responds quickly to the RoCoF, disturbance/distortion rejection, and noise immunity to the grid. In recent literature, the effect of the PLL dynamics on a weak grid has been of great concern because of its unmodeled dynamics that destabilize the converter under the weak-grid condition. This thesis proposes showing the impact of the weak-grid on the VSC as the dynamic of the grid changes. It also provides remedies to the grid instability and high-power injection levels. The detailed

PLL dynamics model, including the ac-bus voltage dynamics with constant frequency, is developed and linearized. Even at a fixed frequency, there are various factors that play a role in grid instability, and this tremendously affects the ability of the VSC to control the grid efficiently. The effect of the PLL gain under the weak-grid condition is analyzed.

INDEX WORDS: Phase-locked loop dynamics, Low-inertia grid, Voltage-source converter (VSC), Weak grid.

PHASE-LOCKED LOOP CONTROL IN LOW-INERTIA GRID-CONNECTED VOLTAGE-SOURCE CONVERTERS

by

IFECHUKWUDE ODOGWU

B.S., Georgia Institute of Technology, 2017

M.S., Georgia Southern University, 2020

A Thesis Submitted to the Graduate Faculty of Georgia Southern University in Partial Fulfillment of the Requirements for the Degree

MASTER OF SCIENCE

PHASE-LOCKED LOOP CONTROL IN LOW-INERTIA GRID-CONNECTED VOLTAGE-SOURCE CONVERTERS

by

IFECHUKWUDE ODOGWU

Major Professor:	Masoud Davari
Committee:	Rocio Alba Flores
	Weinan Gao
	Seungmo Kim

Electronic Version Approved:
July 2020

DEDICATION

This thesis is dedicated to my friends and family for their support. I am most grateful to God Almighty for his continuous blessings and to my colleagues for their technical and intellectual support.

ACKNOWLEDGMENTS

I want to acknowledge Dr. Masoud Davari for the guidance and support he provided throughout the duration of my master's program. His supervision has been pertinent to the successful completion of my thesis work. I appreciate his time, efforts, ideas, and financial support during my program. I want to express my gratitude to Dr. Rocio Alba Flores, Dr. Weinan Gao, and Dr. Seungmo Kim for the time contributed to being a part of this thesis committee. I would also like to acknowledge Tri Nguyen, Mohammed Mynuddin, and Yakub Sharif for the research guidance, knowledge, and assistance they provided, which enabled me to complete my research. Last but not least, I would also like to acknowledge the financial support of the U.S. National Science Foundation (NSF), through Grant #1808279, provided by the Core Program of Energy, Power, Control, and Networks (EPCN) in the Division of Electrical, Communications and Cyber Systems (ECCS).

TABLE OF CONTENTS

Page

LIST OF TABLES

Page

LIST OF FIGURES

Page

LIST OF SYMBOLS

Symbol	Description	Symbol	Description
θ	Phase angle	ρ	Angular position
ω	Angular velocity	ω_g	Angular velocity of the grid
$\Delta\omega$	Difference of nominal and grid angular velocity	ζ	Damping factor
S	Apparent power	P	Active power
Q	Reactive power	R	Connection Resistance
L	Filter inductance	C_f	Filter capacitance
I_d	d-axis component of current	I_q	q-axis component of current
V_d	d-axis component of voltage	I_q	q-axis component of voltage
K_P	Proportional gains	K_I	Integral gains

CHAPTER 1

INTRODUCTION

1.1 BACKGROUND

With society looking to reduce the carbon footprint generated by the consumption of fossil fuels and the release of CO_2 emissions, there has been a surge in the discovery of alternative means to supply clean, sustainable, and reliable power to the grid. Modern grids thereby have higher penetration from renewable energy sources to accommodate the demand for power and CO_2 emission reduction.

The distributed generation microgrid is a topic of great interest because it provides a solution to the environmental emission, asynchronous interconnection, and diversifies the utility of the grid by providing dc [1]–[4], ac [5], and hybrid ac/dc [6]–[8] power control and utilization. Examples of the diversity it brings to the grid is its provision of direct power supply to dc loads such as electric vehicles, communication, and data centers, along with light-emitting diodes. Power quality factors could be improved, and fewer transformers are needed in the utility grid, improving the cost, size, and efficiency of power transfer [9]–[14].

All these advancements are made possible due to power electronics. One significant power electronic that enables the interconnection of the dc and ac grids, is the VSC. Although these benefits are exciting, they also provide some challenges to the existing grid structure, which is further discussed [13], [14]. The problem with this approach is that as more power from renewable energy resources are integrated, there is evidence that the stability is compromised due to the low-inertia of the grid [15], [16].

One of the significant problems to grid integrity is the rate of change of frequency (RoCoF). RoCoF disturbance caused by generator trip, load rejection, and short circuit fault is usually accommodated by rotational inertia of synchronous generators (SG) in older

grids [17]. The dynamics of the synchronous generator are designed to absorb energy from the grid when there is an increase in frequency and transient grid active power. It stores this excess power as kinetic energy by increasing the SG speed [18]. When there is a shortage of active power and a fall in grid frequency, the SG compensates for this by decreasing the rotor speed as the kinetic energy is released to the grid to provide stability [18]. Modern power systems have low mechanical inertia to combat the RoCoF, so there is more probability for instability [19].

The voltage-source converter (VSC) plays an essential role in both transmission and distribution of power, by being responsible for the efficient transfer of power between the ac and dc networks. The VSC connected grid can then separate into the ac and dc sides. Due to grid duality, the dc energy source, such as the solar and wind farm along with dc loads such as the electric car, communication, and data center, can be connected to the dc side of the grid [14]–[20].

VSC control operation performance under unbalanced and distorted grid conditions is based on its fast, reliable, and accurate synchronization. Synchronization can either be open-loop or closed-loop synchronization [21]. The synchronization method dictates distortion rejection, frequency adaptivity, structural simplicity, and phase-angle adaptivity to guarantee a high-quality operation of the VSC. Open-loop synchronization is built on the knowledge that voltages are in-phase and orthogonal to the grid voltage [22]. It directly estimates the magnitude, phase, and frequency of an incoming signal. An example of the open-loop synchronization is the low-pass filtering (LPF) technique and the space vector filtering (SVF) technique. The drawback to this method is its sensitivity deviation of the grid frequency, its lack of precise adjustment, and high sensitivity to noise and harmonics. The closed-loop synchronization method is a more common approach because of its accuracy. It regulates an error signal to zero due to its feedback loop. A well-known closed-loop method is the phase-locked loop (PLL) system [22]–[24].

1.2 MOTIVATION

RoCoF is just one of the factors that affect grid stability and performance. Another factor that contributes to instability is the grid impedance to the VSC. A couple of factors lead to an increase in grid impedance, but one of such is the control scheme selected together with the PLL implemented.

The PLL dictates the location of poles and zeros that manipulates the open-loop output impedance. The PLL parameters that govern this location are the loop filter gains, K_p, and K_i. Short circuit ratio (SCR) is a tool used to categorize grid impedance between a strong or weak grid. The larger the values of SCR, the stronger the grid stability. A reliable grid is ideal for grid performance and stability. The SCR values work together with the PLL parameters to ensure VSC stability. Higher SCR values are resilient to PLL gains, but lower values are vulnerable to substantial PLL gains. The relationship between PLL gains to specific SCR values plays a significant role in VSC and the entire grid stability. A large grid impedance would undermine the output impedance of the VSC and control performance. This relationship would be analyzed in this work because it is relevant to control the performance of distributed generation.

This work is of high relevance when sizeable renewable energy sources are connected to a preexisting grid to increase power supply. Wind and solar farms are located away from the loads, meaning they have to be connected to the preexisting grid to serve their purpose. The control scheme and facilities of these grids may not accommodate this change. Facilities would have to be upgraded, costing time and money. Understanding the condition of a grid also enables the engineers to decide either between a line-commutated converter (LCC) or a VSC.

1.3 Objective and Scope

This study would improve the design capability of the distribution generation (DG) power electronics to counter the change in grid impedance, transitioning to various steady-state to connect and reconnect to the system without disrupting the power supply.

1.4 Thesis Organization

The remainder of the thesis is organized as follows. Chapter 2 presents the literature relevant to the research and current work. It also presents the two major categories of HVDC, which are discussed with emphasis on VSC. The concept of a weak grid is introduced, and its importance to this literature is stressed. Stability evaluation and phase-locked loop design is presented. In Chapter 3, the dynamic model is proposed for analysis and simulation. Results and discussions are presented in Chapter 4. First, the active and reactive power stability is presented. Next, the simulation of the system stability at various K_p gains are depicted on a pole map to investigate grid stability. Chapter 5 concludes the thesis with a summary of the present work and the scope of future works are briefly outlined.

CHAPTER 2

LITERATURE REVIEW

2.1 HIGH-VOLTAGE DIRECT CURRENT

HVDC converters are very popular because they provide bi-directional power supply, converting high voltage alternating current (ac) to direct high-voltage current (HVDC) called rectification. It can do otherwise, which is known as inversion [25]. This property permits efficient power flow from where it is needed to where it is abundant. It saves the cost of operation and ensures the power balance in the system. In distributed energy sources such as solar farms, it provides system functions such as real and reactive power regulation, voltage and frequency support during islanding conditions. Line-commutated and voltage-source converters are two significant categories of HVDC converters.

2.1.1 LINE-COMMUTATED CONVERTER

In LCC, the reversal of current flow is only possible when the polarity of the voltage on both stations is reversed [25]. It is a standard configuration because it is older and well established compared to its counterpart. The configuration utilizes thyristors for switching, which only offers one degree of control because switches can only be turned on. This configuration introduces sizable harmonic distortion, which needs significant filtering. Another drawback to this configuration is that it requires additional equipment for a black start. Apart from its site size and other drawbacks, its high power capability, low station losses, high reliability, and excellent overload capability are features that make it of high demand in the industry.

2.1.2 VOLTAGE-SOURCE CONVERTERS

It is a modernized version of an LCC because it utilizes an insulated-gate bipolar transistor (IGBT). It provides two degrees of freedom enabling improved harmonic filtering and creating more exceptional reactive power control with fewer filters.

There are three major types of VSC connections. They are grid-imposed frequency VSC system, controlled-frequency VSC system, and variable-frequency VSC system. Grid-imposed frequency VSC systems are typically interfaced with a relatively sizable stiff utility ac system. Therefore, the operating frequency is constant and dictated by the ac system. Controlled-frequency VSC are converters with control schemes that regulate the ac system frequency. Its reference frequency may be obtained from a supervisory control system. In the variable-frequency VSC system, the converter is interfaced with an electric machine, and the operating frequency is a state variable of the overall VSC system. VSC is marketable because it serves a significant role in interconnecting a weak grid. It has a compact site size and is used with conventional transformers.

VSC is often sought in DG because it can perform when connected to a weak grid. It has the ability to self commutate at specific SCR values. Stability can be preserved when active power injection capability is reduced to 0.5–0.6 per unit (pu) under SCR as low as 1 [26]. The significant risk to VSC is commutation failure because it changes the output of the VSC. Other risks associated with extremely weak grids are high temporary overvoltages, voltage instability, low-frequency resonances, and long fault recover times [27].

2.1.3 TWO-LEVEL CONVERTER

Like the LLC configuration, the two-level converter has IGBT and inverse-parallel diodes in place of thyristors to improve controllability. It comprises six valves with two

valves corresponding to one phase of the ac output. The two halves which make a half-bridge are turned on simultaneously to avoid uncontrolled discharge of the capacitor [28].

It provides a bidirectional power-flow path between the dc-side and the three-phase ac system. It can also be controlled in $\alpha\beta$-frame and dq-frame. Although this sounds great compared to the LLC, its operation accompanies a lot of harmonic losses due to high switching loss. These losses can be reduced with more switches but that would increase costs.

2.1.4 THREE-LEVEL CONVERTER

The need to achieve higher voltage switching and improve the poor harmonic performance has led to the development of a multilevel converter with improved harmonic performance for utility and high power applications [29], [30]. The typical configuration is a neutral-point-clamped (NPC) or sometimes diode-clamped converter. Each phase in this topology contains four IGBT valves with ratings to withstand half of dc line-line voltage and two clamped diode valves [31]. It provides a better three-phase ac voltage with lower harmonics.

2.2 WEAK GRID

Grid strength is measured either with short circuit ratio or inductive-resistive ratio (IRR). SCR is defined as a Thevenin representation of the approximate estimation of the system. It does not serve as a full system analysis but provides an insight into the equivalent impedance to the source. SCR can be defined mathematically as the ratio of short circuit level to that of the terminal power. It can also be defined as the ac system per unit admittance of the dc power. This ratio is important because when this value is low, it introduces harmonic distortion, voltage fluctuation, varying frequency, line overload, and voltage variations [32], [33]. Reactive power supplied from the VSC can also affect the SCR, but some

solutions used in the industry to solve these problems are capacitor banks, synchronous condensers, synchronous compensators (SC), and static var compensator (SVC) [34].

Analysis from [27] shows that the grid becomes weaker using SVC but provides quick response to over-voltage. SC improves SCR but has a slower response. This paper considers combining SVC and SC to take advantage of its benefits, which seem appropriate, but more substantial voltage levels and loads would require a lot of expensive compensations.

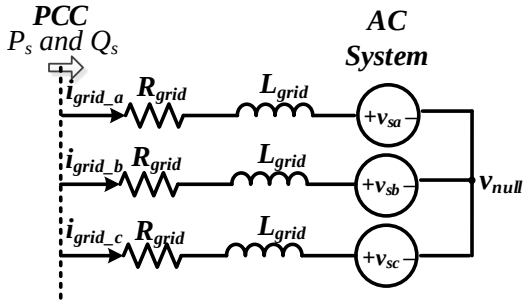

Figure 2.1: Power Flow

The SCR has an inverse relationship with the impedance of the grid Z_{grid}. This impedance comprises load, voltage regulators, line impedance, and the internal impedance of the input. Stiffer grid has more excellent power transfer capability because the transfer power is inversely proportional to the amplitude between the PCC and the grid, as illustrated in (2.1). The first term of (2.1) represents the relationship between the power flow and the load angle. If V_{pcc} and V_{grid} are assumed to be 1.0 pu at steady-state operation the difference between δ and α_z, which is the converter's load angle cannot be greater than $90°$ at steady-state given that at $90°$ it is at its theoretical limit. The second term is the active power dissipated in the equivalent resistance between the PCC and the grid. Another factor that affects grid stability which would be intensively discussed in this work is the PLL in a weak-grid condition.

$$P_{12} = \frac{V_{\text{pcc}} V_{\text{grid}}}{|Z_{\text{total}}|} \sin(\delta - \alpha_z) + \frac{V_{\text{pcc}}^2 R_{\text{total}}}{|Z_{\text{total}}|^2} \tag{2.1}$$

$$\alpha_{\text{z}} = \text{arctg}\left(\frac{R_{\text{total}}}{X_{\text{total}}}\right) + \frac{V_{\text{pcc}}^2 R_{\text{total}}}{|Z_{\text{total}}|^2}$$

and δ is the load angle [35].

2.3 Evaluating System Stability

Stability in the ac system can be classified but not bound to small-signal stability, sub-synchronous resonance, mid-to-term stability, and transient stability [36]. This stability analysis is dependent on the source of power, and the amount of power delivered.

The PLL's contribution to the operating point's power system stability cannot be overstated due to its role in maintaining synchronization during a disturbance.

- *Small-Signal Stability:* The stability analysis of this thesis is based on the small-signal model. It is the ability of the power system to be synced during small disturbances. Without synchronous generators in a modern distributed system, disturbance is limited to insufficient damping of systems oscillations [36]. This is due to the power electronics connecting the source to the grid. Small-signal stability can be examined by an understanding of the components characteristic dynamics and equation providing sufficient information for modeling.

- *Transient Stability:* As earlier discussed in chapter 1, on the role of synchronous generators in maintaining reference voltages and angles under transmission faults, transient disturbance, and low generation. The synchronous generator dynamics is well studied to guarantee grid stability. In the same way, the converter in this work ensures the adequate control schemes to safeguard grid strength.

- *Sub-Synchronous Resonance Stability:* Sub-synchronous resonance stability is done for extensive ac systems such as hydropower or coal plants, which typically generate hundreds of megawatts. This stability would not be discussed further in this work.

- *Mid-to-Long Term Stability:* This stability is concerned with power flow from the generation to load regulated by the VSC. It is also considered for DG operation in islanding mode [36].

In a large grid, they are many factors that determine grid stability that vary from voltage control, current control, and PLL. This parameter provides the control scheme that shapes the VSC impedance to ensure grid stability. The focus of this thesis would be to outline the effect of the output impedance due to the PLL dynamics.

2.4 PHASE-LOCK LOOP DESIGN

There are four major outline specifications in designing a basic PLL for accurate frequency and phase-lock [37].

- *Hold Range $\Delta\omega_H$:* This is the range of frequency where the PLL can maintain phase-lock constantly. There is no phase-lock when input frequency exceeds this range.

$$\Delta\omega_H = K_{\mathrm{PD}} K_{\mathrm{VCO}} LF(0) \tag{2.2}$$

  where K_{PD} is the gain of the phase detector. K_{VCO} is the gain of voltage controlled oscillator and $LF(0)$ is the dc gain of the loop filter.

- *Pull-in Range $\Delta\omega_P$:* The pull-in range of frequency is when the PLL is locked into the phase angle of the input signal. T_P is the pull-in time needed by the PLL to become locked.

$$T_P = \frac{\pi^2}{16}\frac{\Delta\omega_n^2}{\zeta\omega_n^3} \tag{2.3}$$

where ζ is the damping factor and ω_n is the natural frequency.

- *Pull-out Range* $\Delta\omega_{\mathrm{PO}}$*:* The pull-out range is smaller than the hold range. This is the range of stability operation of a PLL. Out of this range, the PLL loses tracking and falls into the hold range.

$$\Delta\omega_{\mathrm{PO}} = 1.8\omega_n(\zeta + 1) \tag{2.4}$$

- *Lock Range* $\Delta\omega_L$*:* This is the best range for the PLL. At this range, the PLL will be locked quickly in this range. Utilizing a PI filter, the lock range can be calculated with the equation below.

$$\Delta\omega_L = 2\zeta\omega_n = 2\zeta\sqrt{K_pK_i} \tag{2.5}$$

The relationship and operation of these specifications can be best summed up below.

$$\Delta\omega_L < \Delta\omega_{\mathrm{PO}} < \Delta\omega_P < \Delta\omega_H$$

There are various control schemes used in DG, such as sliding mode control, nested-loop dq control, and direct power control. The use of the control schemes depends on the system and its intended application. The focus of this thesis is the PLL dynamics that employ the nested-loop dq-frame control.

2.5 PHASE-LOCKED LOOP

The criteria in designing a closed-loop system is that it provides fast-tracking and excellent filtering characteristics. A PLL is a negative feedback system, as illustrated in

(3.1), which consists of a phase detector (PD), that measures the phase difference between the input signal and the desired signal created by the voltage-controlled oscillator (VCO). This output is then passed to the loop filter (LF), the proportional-integrator (PI) controller, to cut off the noise signal. It has to accurately estimate the phase angle of the grid voltage, ensuring the correct generation of the reference signal, system stability, and accuracy of the systems control loop. Signal is sent to the control system to determine the switching signal of the converter. The value from LF is used as input to the VCO to create once again the desired signal wave, which is typically 60Hz sine wave. Apart from the power grid, it is utilized in electronics and in communication to match an existing signal in phase with its internal oscillator.

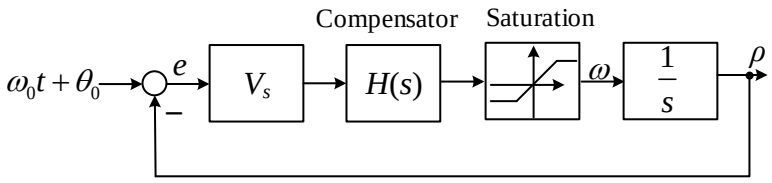

Figure 2.2: PLL Control Block

Limitations to the PLL dynamics such as frequency adaptivity, unbalance robustness, and distortion rejection have led to more research to enhance the performance or create better synchronization methods. These limitations have introduced recent research on enhancing its performance. A recent work on the extended three-phase PLL-based method, accommodates the unbalanced voltages. The innovation in this method is the replacement of all-pass filters with extended phase-locked loops, which are adaptive notch filters. Its frequency mirrors the grid center frequency, thereby reducing the sensitivity of frequency variation, and due to its band-pass filter, it extracts the positive sequence with no distortion [22].

2.6 CONTROL TECHNIQUE

VSC's efficient use involves an understanding of its intended application and determining what control methodology is most appropriate. Some of these control schemes used in industry are sliding mode control [38], direct power control [39], and the most popular, is the nested-loop direct-quadrature (dq) current control [28], [40].

2.6.1 SLIDING MODE CONTROL

The sliding mode control (SMC) is designed for nonlinear systems. It is used for systems where the plant model cannot be accurately derived or is not needed for the control design. The control scheme operates by switching/sliding between boundaries of different continuous structures based on the current position of the state space [38], [41]. Therefore, it is known to be a variable structure control. It is applied in VSC because it offers better stability notwithstanding load or plant parameters [42], [43].

2.6.2 DIRECT POWER CONTROL

This is an alternative to the conventional vector control. It regulates the active and reactive power without the use of the current control loop [39], [44], [45]. It is easy to implement and offers a simple structure with direct control capacity of the active and reactive power [46], [47].

2.6.3 NESTED-LOOP DIRECT-QUADRATURE CURRENT CONTROL

Conventional control in the dq-frame is based on the nested-loop dq control scheme, which generally includes an outer control loop, either power control or dc voltage control, and an inner current control loop [40]. This control requires a frame of reference transformation. The ac voltage/current is transformed into their respective dq quantities via Park's

transformation. The outer control loop generates the respective dq current references while the inner control loop regulates the dq currents and generates the appropriate switching pulses for converters.

The VSC adopts two proportional-integral (PI) controllers for the inner controller and two outer controllers for the dc-link and ac-bus voltage control. The dc-link controller generates the d-axis reference frame while the ac-bus generates the q-axis reference current component. The benefit of this control scheme is that it regulates the dc-link and ac-bus voltage and decides the injection and absorption of reactive and active power. This advantage provides both PQ bus control and PV bus control [48].

CHAPTER 3

SYSTEM MODEL

A 30kVA, 500V (in dc), 260V (in ac), 60Hz, weak-grid connected bidirectional VSC is shown in Figure 3.1. It depicts a lossless power processor with a dc bus capacitor $C_{DC_{\text{eq}}}$, a current source on the dc side modeling the power loss p_{loss} due to fast recovery and tailing current of the power switches.

Parameter	**Value**
VSC DC Source	500 V
Base Voltage	260 V
System Frequency	60 Hz
Filter	$\mathrm{R} = 0.01\ \Omega, \mathrm{L} = 2.4\ \mathrm{mH}, \mathrm{C} = 1\ \mu\mathrm{F}$
Switching Frequency	8100 Hz
VSC Capacity	30 kVA

Table 3.1: System Parameter

The dc side of the VSC is interfaced with each phase with the ac system. The ac system V_{sabc} is a sinusoidal signal. An L-based filter is implemented by the L representing the transformer leakage inductance and the filter, while R is the equivalent resistance. The internal loss is modeled by r_{on} and resistance R commonly adopted in high-power converters.

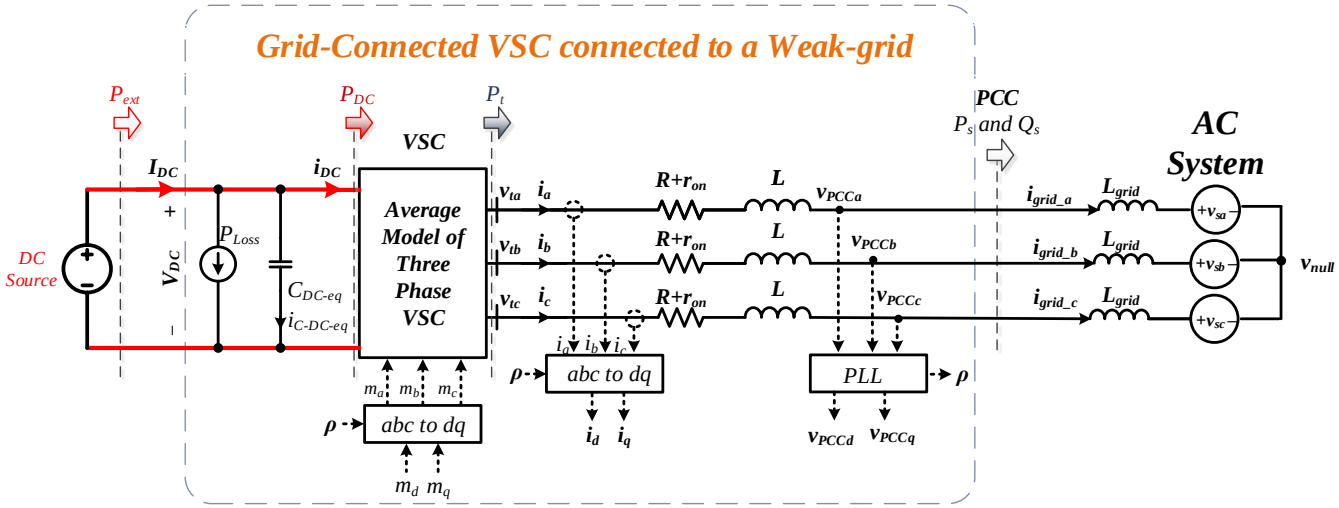

Figure 3.1: VSC Connected weak ac Grid

The ac system equivalent model is analyzed by its Thevenin's equivalent circuit viewed from the PCC. The internal voltage is represented by V_s and grid inductance by L_{grid}. The system parameters can be seen in Table 3.1. The ac grid and the dc grid dynamics cannot be combined together to design the converter dynamics because it makes the design more ambiguous. Therefore as stated in [26], [49]–[52], the equivalent model is obtained from the ac grid observed from the point of common coupling (PCC) for the design and analysis. The ac grid is mainly represented by the L_{grid} because the grid is mainly inductive, especially when viewed from the sub-transmission or transmission levels. The ac system voltage in the VSC system of Fig. 3.1 is expressed as below.

$$V_{sa}(t) = \widehat{V}_s \cos[\omega(t)] \tag{3.1}$$

$$V_{sb}(t) = \widehat{V}_s \cos\left[\omega(t) - \frac{2\pi}{3}\right] \tag{3.2}$$

$$V_{sc}(t) = \widehat{V}_s \cos\left[\omega(t) - \frac{4\pi}{3}\right] \tag{3.3}$$

$\widehat{V}_s$ is the peak value of the line-to-neutral voltage. The source ac system frequency ω_0 and θ_0 is the initial phase angle of the source.

$$\vec{V}_s(t) = \widehat{V}_s e^{j(\omega_0 t + \theta_0)} \tag{3.4}$$

Symmetrical three-phase system can be described by a complex-valued function called space-phasor equations, as seen in (3.4). Space-phasor equation can be expressed in polar coordinates. It is essential when the magnitude and phase of a system dynamics are of interest.

Dynamics of the ac side

$$L_{grid}\frac{d\vec{i}_{grid}}{dt} = \vec{V}_{pcc} - \vec{V}_s \tag{3.5}$$

Substituting $\vec{V}_s$ from (3.4) in (3.5)

$$L_{\text{grid}}\frac{d\vec{i}_{\text{grid}}}{dt} = \vec{V}_{pcc} - \widehat{V}_s e^{j[\omega_0 t + \theta_0]} \tag{3.6}$$

For control design implementation, it is essential to map the space-phasor equation in the cartesian coordinate system, where one deals with real-valued functions of time. This is known as $\alpha\beta$-frame control. In order to achieve zero steady-state error in the $\alpha\beta$-frame control, the bandwidth of the closed-loop system must be adequately more significant than the ac system frequency. After mathematical manipulation, the dq-frame representation of the ac-side dynamics is described in (3.7) and (3.8)

$$L_{grid}\frac{di_{grid_d}}{dt} = L_{grid}\omega(t) i_{grid_q} + V_{pcc_d} - \widehat{V}_s \cos[\omega_0 t + \theta_0 - \rho] \tag{3.7}$$

$$L_{grid}\frac{di_{grid_q}}{dt} = -L_{grid}\omega(t)i_{grid_d} + V_{pcc_q} - \widehat{V}_s \sin[\omega_0 t + \theta_0 - \rho] \tag{3.8}$$

$$\frac{d\rho}{dt} = \omega(t) \tag{3.9}$$

In the dq-frame control, zero steady-state error is readily achieved by including integral terms in the compensator given the control variables are dc quantities. The real and reactive power are controlled in dq-frame, where VSC and the grid become proportional to the d and q-axis, respectively. Compared to the $\alpha\beta$-frame control, the dq-frame control requires a synchronization mechanism that is achieved through the phase-locked loop. $\rho(t)$, which is the synchronization mechanism, utilizes the phase angle to govern the adjustment of the rotational speed of the dq-frame [18].

3.0.1 PHASE-LOCKED LOOP

$$L_{grid}\frac{di_{grid_d}}{dt} = L_{grid}\omega(t)i_{grid_q} + V_{pcc_d} - \widehat{V}_{max} \cos(\omega_0 t + \theta_0 - \rho) \tag{3.10}$$

$$L_{grid}\frac{di_{grid_q}}{dt} = -L_{grid}\omega(t)i_{grid_d} + V_{pcc_q} - \widehat{V}_{max} \sin(\omega_0 t + \theta_0 - \rho) \tag{3.11}$$

$$\frac{d\rho}{dt} = \omega(t) = H(p)V_{PCC_q}(t) \tag{3.12}$$

When ρ converges to $\omega_0 t + \theta_0$ under perfect synchronization, the q-component of the grid voltage at PCC [i.e., $V_{sq} = V_s \sin(\omega_0 t + \theta_0 - \rho)$] will be zero. The PLL dynamics are included in the ac-bus voltage dynamics because during a transient, especially in weak-grid condition, perfect synchronization is not achieved. In dq three-phase PLL, the rate of change of synchronization angle or estimation frequency $\omega(t)$, is developed by the q-component of the grid voltage at the PCC [i.e., $V_{pcc_q}(t)$] together with a PLL filter with a

transfer function $H(s)$ as illustrated in (3.11) and (3.12). The PLL filter can either be a PI or PID controller.

The system dynamics of (3.10) to (3.12) are nonlinear and would have to be linearized to develop a controller. The nonlinear dynamics is linearized around an equilibrium point depicted in (3.13). Subscript "0" represents the steady-state operating point, while "$\sim$" is the small-signal perturbed point around the variable. After mathematical deductions, the linearized dynamics can be seen in (3.14) to (3.16) [48], which are represented in the complex frequency domain.

$$\begin{cases} V_{\mathrm{PCC}_d} = V_{\mathrm{PCC_{d0}}} + \tilde{V}_{\mathrm{PCC_d}} \\ V_{\mathrm{PCC}_q} = V_{\mathrm{PCC_{q0}}} + \tilde{V}_{\mathrm{PCC}_q} \\ i_{\mathrm{grid_d}} = I_{\mathrm{grid_{d0}}} + \tilde{I}_{\mathrm{grid_d}} \\ i_{\mathrm{gridq}} = I_{\mathrm{grid_{q0}}} + \tilde{I}_{\mathrm{grid_q}} \\ \omega_0 t + \theta_0 - \rho = -(\rho_0 + \tilde{\rho}) \\ \frac{d\rho}{dt} = \omega_0 + \frac{d\tilde{\rho}}{dt} \Rightarrow \omega = \omega_0 + \tilde{\omega} \end{cases} \tag{3.13}$$

3.0.2 Linearized Phase-Lock Loop Dynamics

The state-space model of the nondynamic V_{pcc_d} is the input variable. $\omega(t)$, and V_{pcc_q} are the disturbance. ρ, i_q, and i_d are state variables.

$$\tilde{V}_{\mathrm{pcc}_d}(s) = L_{\mathrm{grid}} s \tilde{I}_{\mathrm{grid}_d}(s) - L_{\mathrm{grid}} \omega_0 \tilde{I}_{\mathrm{grid}_q}(s) - L_{\mathrm{grid}} (I_{\mathrm{grid}_q 0} s + \omega_0 I_{\mathrm{grid}_{d0}}) \tilde{\rho}(s) \tag{3.14}$$

$$\tilde{V}_{\mathrm{pcc}_q}(s) = L_{\mathrm{grid}} s \tilde{I}_{\mathrm{grid}_q}(s) + L_{\mathrm{grid}} \omega_0 \tilde{I}_{\mathrm{grid}_d}(s) + [L_{\mathrm{grid}} I_{\mathrm{grid}_{q0}} s - (V_{pcc_{d0}} + L_{grid} \omega_0 I_{grid_{q0}})] \tilde{\rho}(s) \tag{3.15}$$

$$\tilde{\rho}(s) = \frac{H(s)}{s} \tilde{V}_{\mathrm{pcc}_q}(s) \tag{3.16}$$

In order to obtain the dynamics of the synchronization angle, (3.15) and (3.16) are combined to deduce (3.17) as seen below.

$$\tilde{\rho}(s) = \frac{H(s)\left[L_{\text{grid}} s \tilde{I}_{\text{grid}q}(s) + L_{\text{grid}}\omega_0 \tilde{I}_{\text{grid}_d}(s)\right]}{\left[s - H(s)\left[L_{\text{grid}} I_{\text{grid}_{q0}} s - \left(V_{\text{pcc}_{\text{d0}}} + L_{\text{grid}}\omega_0 I_{\text{grid}_{q0}}\right)\right]\right]} \tag{3.17}$$

Linearized PCC voltage is obtained by combining (3.17) and (3.14)

$$\begin{aligned}
\tilde{V}_{\text{PCC}_d}(s) =& \frac{P(s)}{s - H(s)R(s)}\tilde{I}_d(s) - \frac{P(s)}{s - H(s)R(s)}\tilde{I}_{\text{Load}_\text{d}}(s) \\
&+ \frac{E(s)}{s - H(s)R(s)}\tilde{I}_q(s) - \frac{E(s)}{s - H(s)R(s)}\tilde{I}_{\text{Load}_q}(s) \\
P(s) =& L_{\text{grid}}\left\{s^2 - \left[sR(s) - \omega_0 D(s)\right]H(s)\right\} \\
E(s) =& L_{\text{grid}}\left\{-\omega_0 s + \left[\omega_0 R(s) - sD(s)\right]H(s)\right\} \\
D(s) =& L_{\text{grid}}\left(I_{\text{grid}_{q0}} s + \omega_0 I_{\text{grid}_{d0}}\right) \\
R(s) =& L_{\text{grid}} I_{\text{grid}_{q0}} s - \left(V_{\text{PCC}_{d0}} + L_{\text{grid}}\omega_0 I_{\text{grid}_{q0}}\right)
\end{aligned} \tag{3.18}$$

The ac-bus dynamics under the weak-grid condition can be represented in (3.18). The third equation represents the plant model. Signal $\tilde{I}_{\text{Load}_q}$ and $\tilde{I}_{\text{Load}_d}$ are treated as a disturbance to the system. $\tilde{I}_d$ and $\tilde{I}_q$ are the two control signals controlled by VSC. $\tilde{I}_d$ regulates the dc-link voltage while $\tilde{I}_q$ is used to control the reactive power [48].

$$\begin{aligned}
\tilde{V}_{\text{pcc}_d}(s) =& \frac{P(s)}{s - H(s)R(s)}\tilde{I}_d(s) - \frac{P(s)}{s - H(s)R(s)}\tilde{I}_{\text{Load}_\text{d}}(s) \\
&+ \frac{E(s)}{(\tau_i s + 1)\left(s - H(s)R(s)\right)}\tilde{I}_q^*(s) \\
&- \frac{E(s)}{s - H(s)R(s)}\tilde{I}_{\text{Load}_q}(s)
\end{aligned} \tag{3.19}$$

τ_i is the time constant of the inner current control loop dynamics modeled by a first-order low-pass filter [53]. The reference q-component of the converter current is $\tilde{I}_q^*(s)$, as shown in (3.19). Under weak-grid conditions, L_{grid} increases, and there is an increase in the coupling of PCC voltage dynamics and the PLL.

$$\frac{\tilde{V}_{pcc_d}(s)}{\tilde{I}_q^*(s)} = \frac{L_{grid}[-\omega_0 s + [\omega_0(L_{grid}I_{\mathrm{grid}q0}s - C) - s(L_{grid}(I_{\mathrm{grid}_{q0}}s + \omega_0 I_{\mathrm{grid}_{\mathrm{d0}}}))]H(s)]}{(\tau_i s + 1)(s - H(s)(L_{\mathrm{grid}}I_{\mathrm{grid}_q}0s - C))}$$

$$C = V_{pcc_d0} + L_{grid}\omega_0 I_{\mathrm{grid}_{q0}} \tag{3.20}$$

Equation (3.20) is the open-loop transfer function of (3.18). This transfer function provides the framework for the numerical analysis in Chapter 4. $H(s)$ is based on the bandwidth criterion for disturbance rejection, and fast-tracking response during voltage unbalance [48].

CHAPTER 4

RESULTS

An understanding of the relationship between the PLL and the impedance of the grid involves linearizing the VSC average model while working on the effects of the nonlinear properties of the PLL. Other research has been done to analyze the relationship between the SCR and PLL, as discussed in [54], which performs a similar study by examining the system's eigenvalues.

4.1 EFFECT OF PROPORTIONAL GAIN

Parameter	**Value**
SCR	2
Grid Inductance	2.1667 mH
Grid Resistance	0.796 Ω
System Frequency	60 Hz
PLL Gain: K_p	180, 100, 50, 20, 1
PLL Gain: K_i	3200

Table 4.1: Stability Analysis of a Weak Grid (SCR=2)

$$\begin{aligned} SCR &= \frac{V_{ac}^2}{SZ_g} \\ Z_g &= R_s + jX_s \\ R_s &= \frac{Z_g}{\sqrt{2}} \\ L_s &= \frac{R_s}{\omega_0} \end{aligned} \tag{4.1}$$

In (4.1), V_{ac} is the base voltage, S is VSC capacity, R_s and L_s are the grid resistance

and inductance, respectively.

4.1.1 Active and Reactive Power Stability

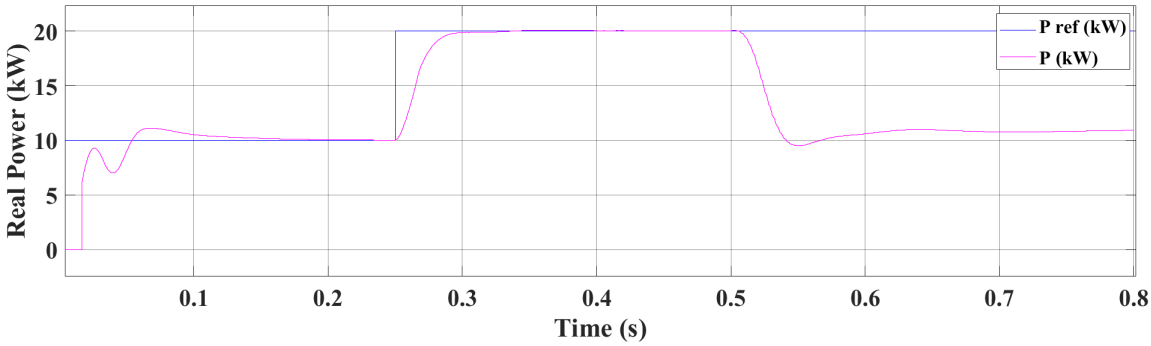

Figure 4.1: Real Power SCR=2 K_p=180 K_i=3200.

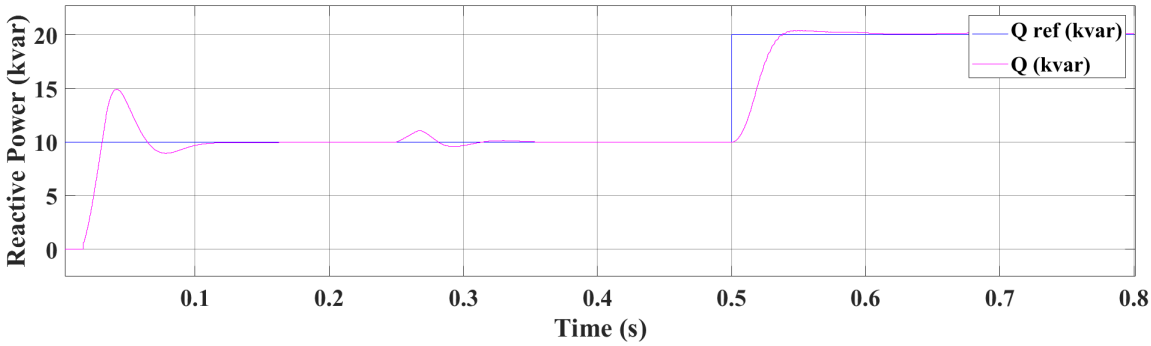

Figure 4.2: Reactive Power SCR=2 K_p=180 K_i=3200.

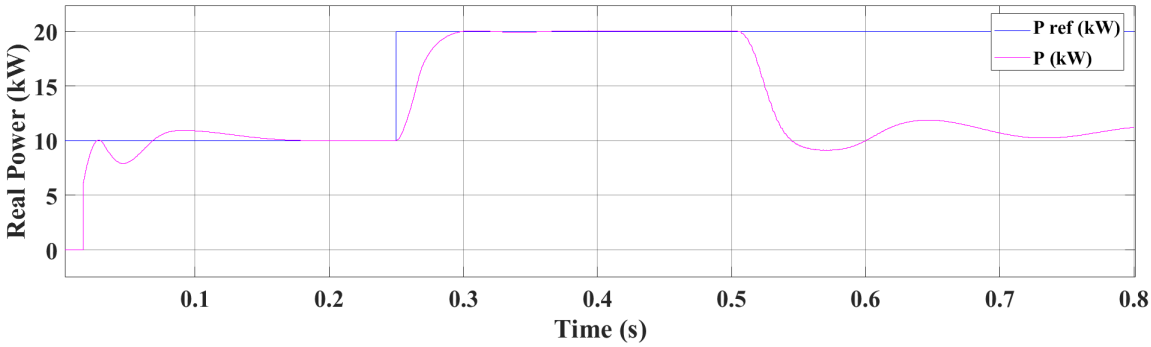

Figure 4.3: Real Power SCR=2 K_p=100 K_i=3200.

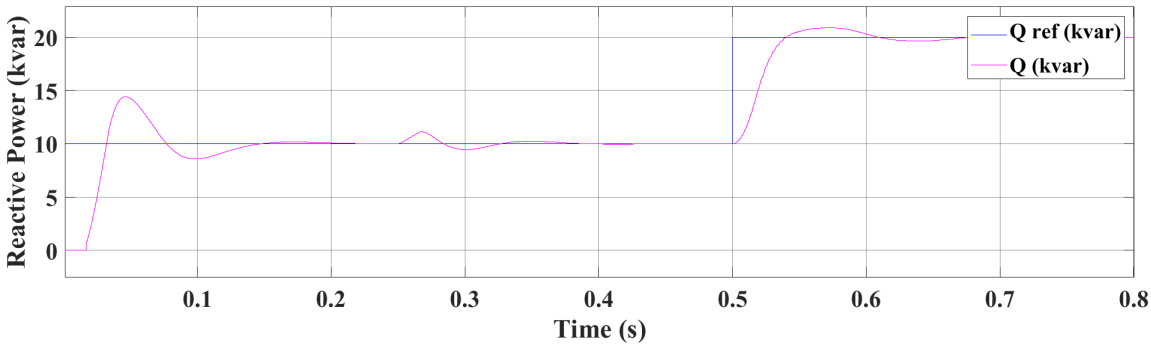

Figure 4.4: Reactive Power SCR=2 K_p=100 K_i=3200.

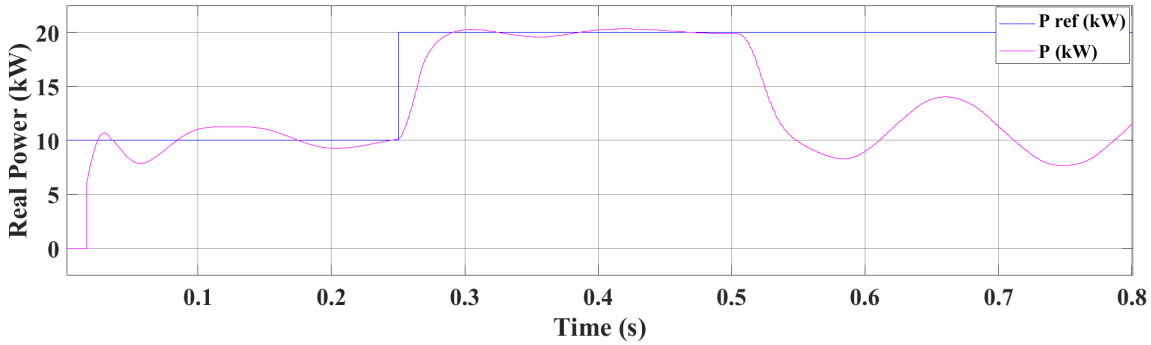

Figure 4.5: Real Power SCR=2 K_p=50 K_i=3200.

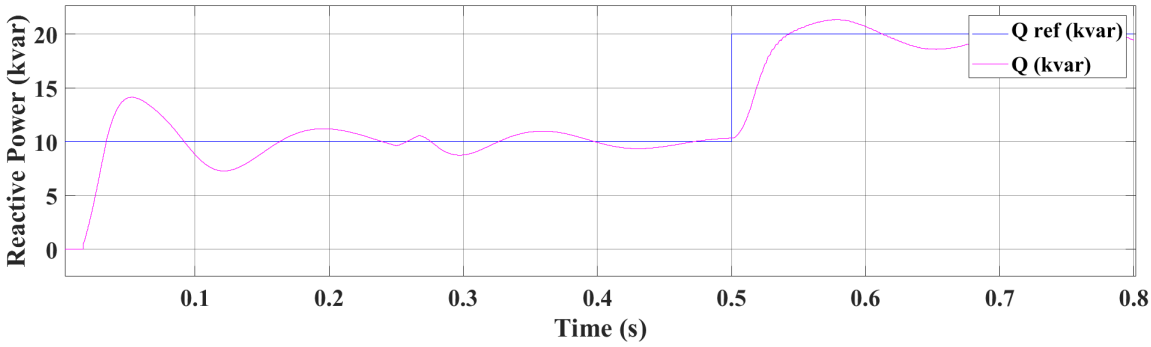

Figure 4.6: Reactive Power SCR=2 K_p=50 K_i=3200.

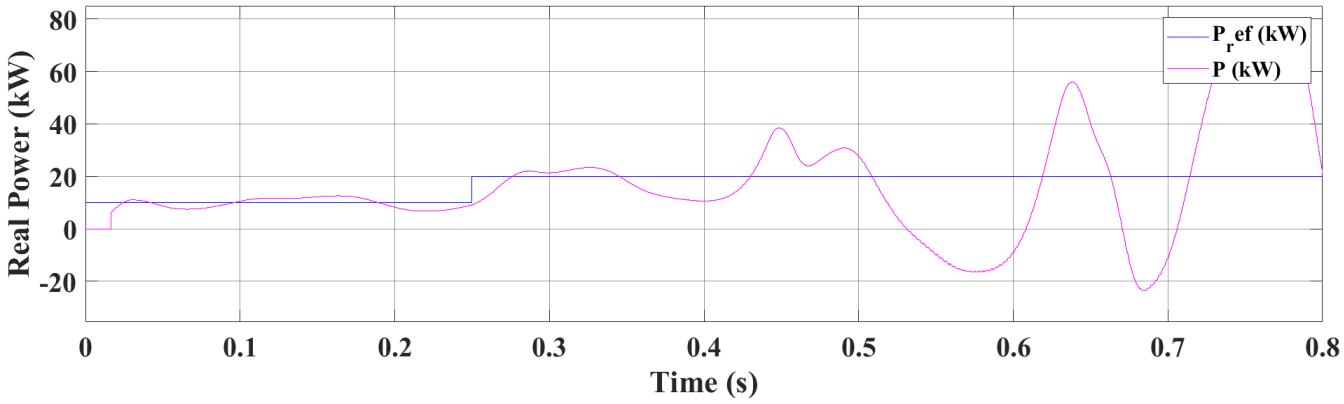

Figure 4.7: Real Power SCR=2 K_p=20 K_i=3200.

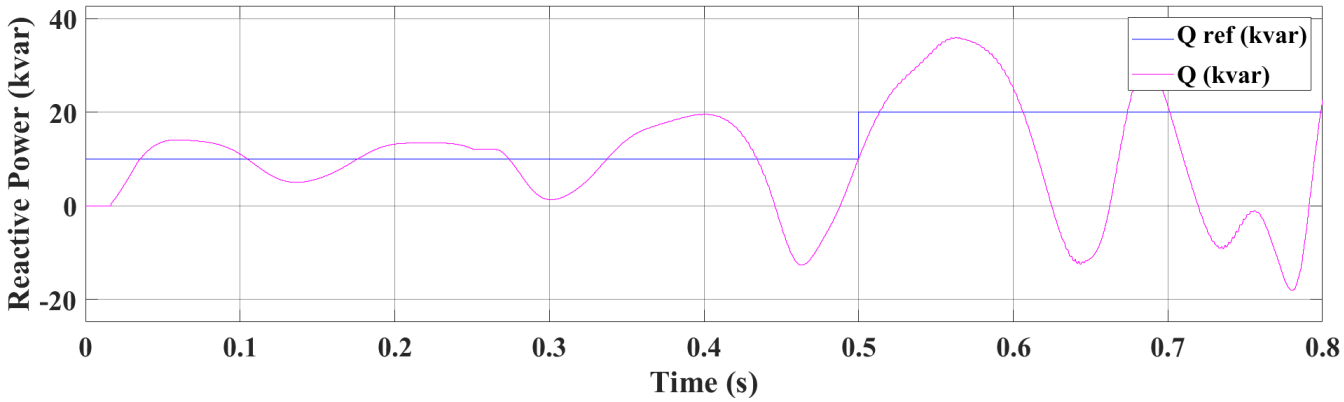

Figure 4.8: Reactive Power SCR=2 K_p=20 K_i=3200.

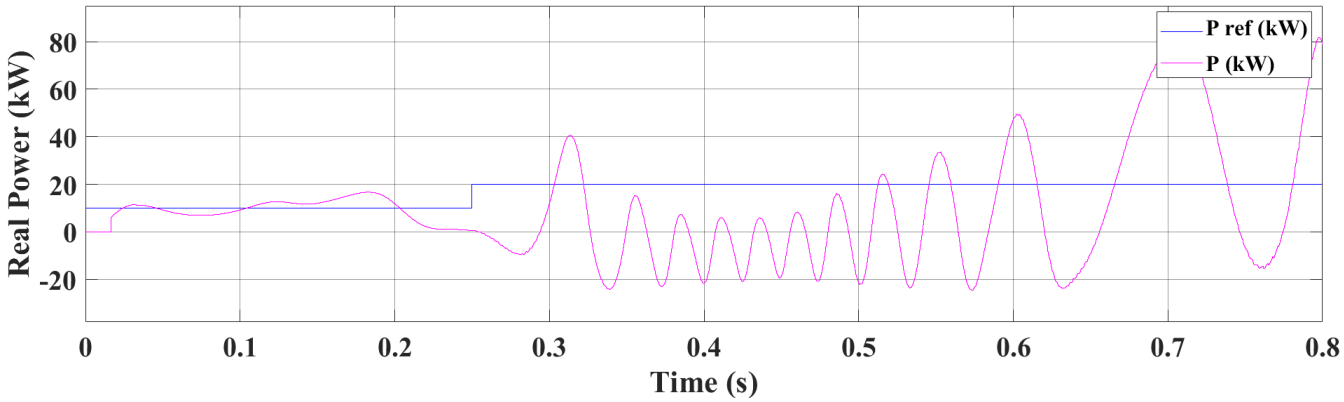

Figure 4.9: Real Power SCR=2 K_p=1 K_i=3200.

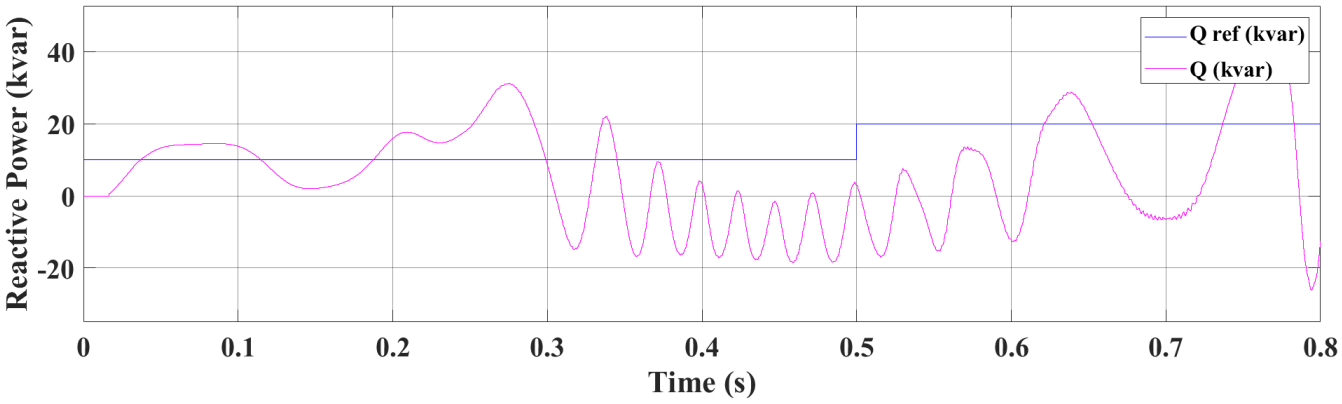

Figure 4.10: Reactive Power SCR=2 K_p=1 K_i=3200.

4.1.2 POLE-ZERO MAP STABILITY

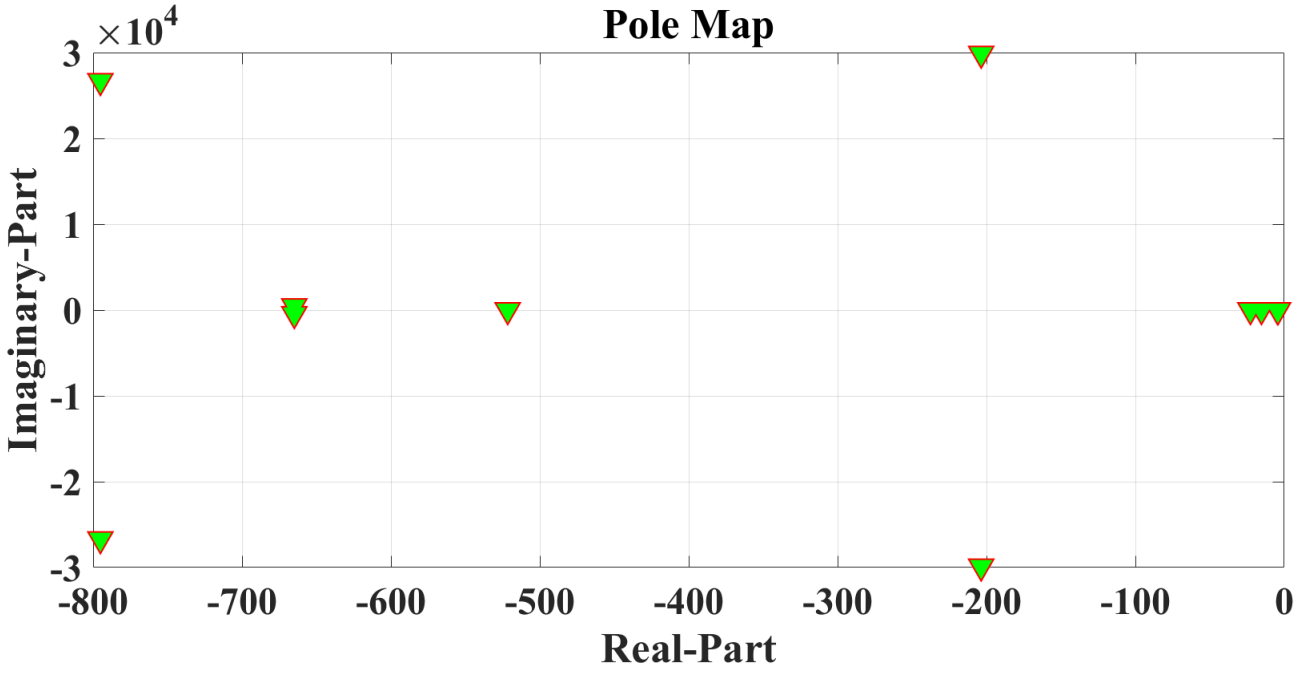

Figure 4.11: SCR=2 K_p =180 K_i=3200.

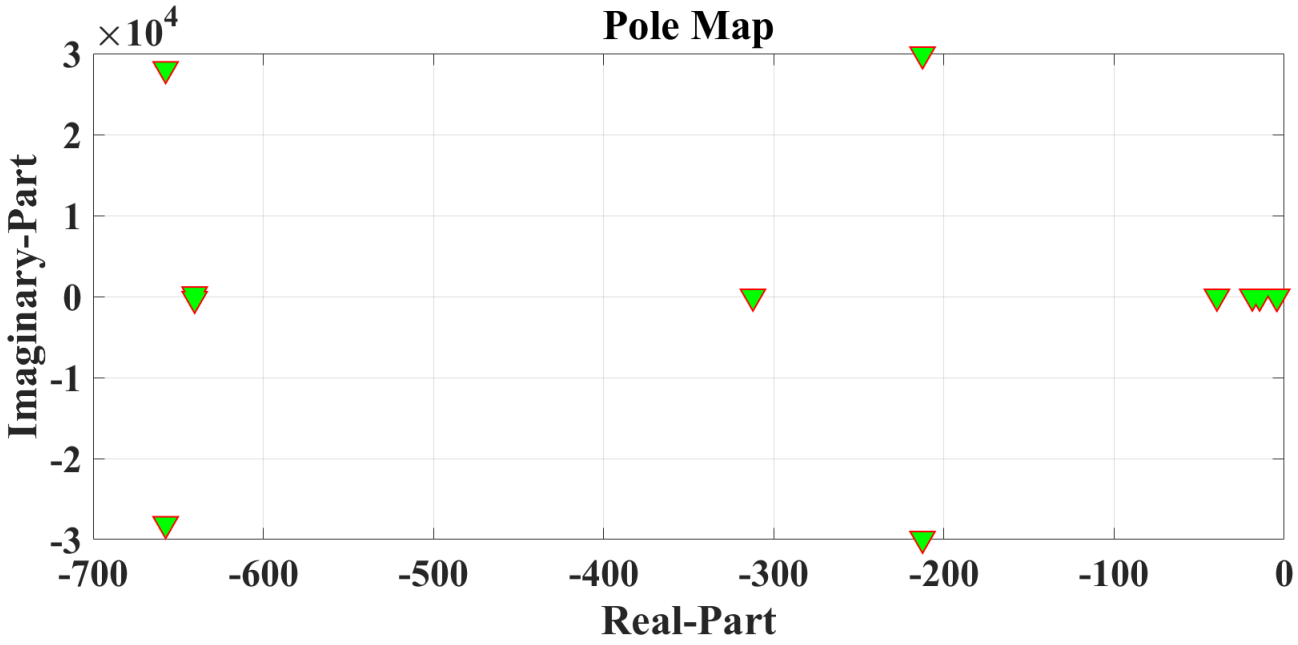

Figure 4.12: SCR=2 K_p=100 K_i=3200.

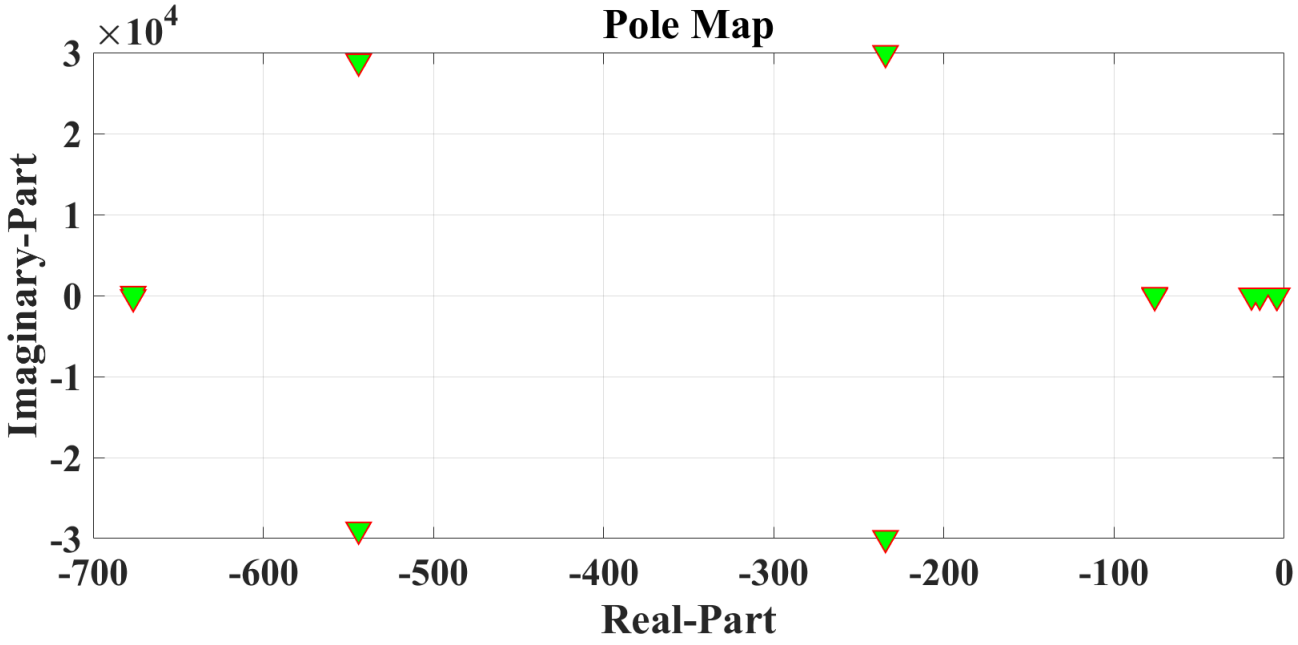

Figure 4.13: SCR=2 K_p=50 K_i=3200.

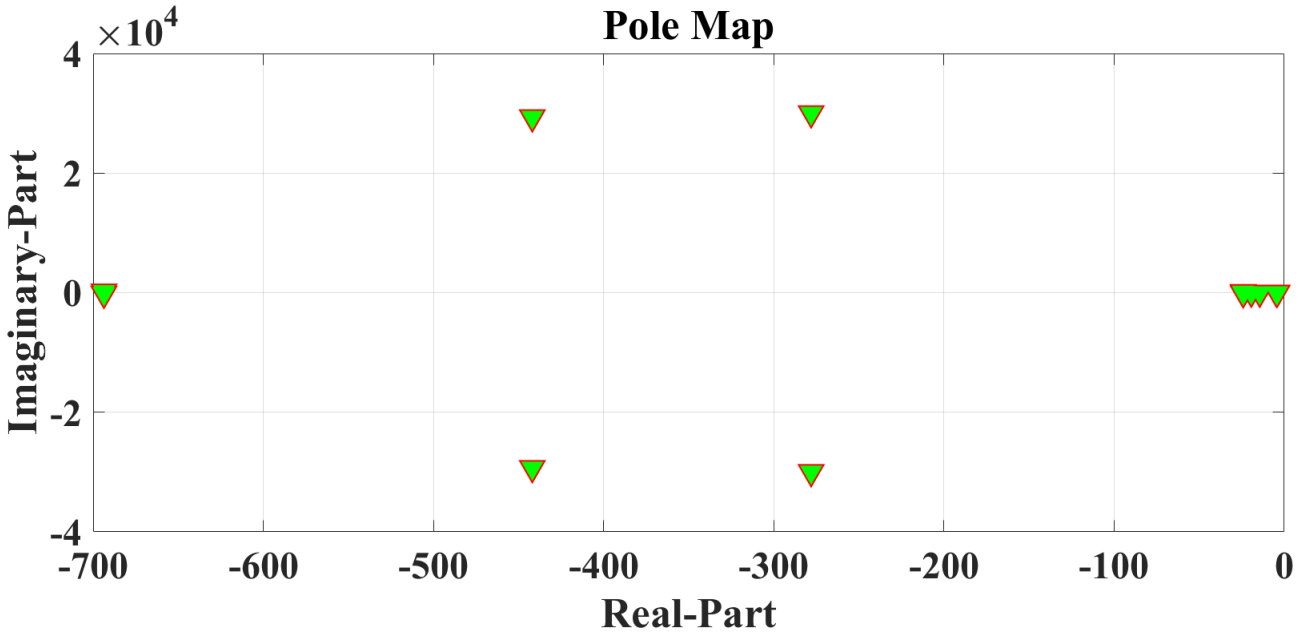

Figure 4.14: SCR=2 K_p=20 K_i=3200.

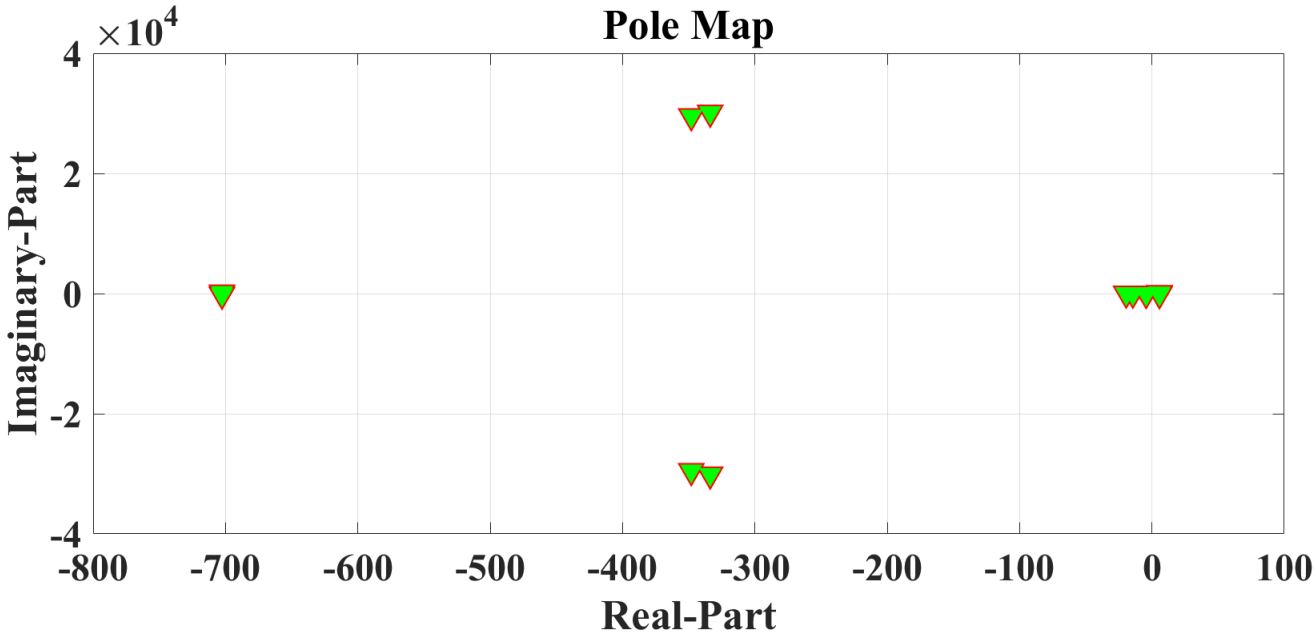

Figure 4.15: SCR=2 K_p=1 K_i=3200.

Matlab Simulink was used to perform this analysis by modeling the system to measure the real and reactive power stability as the K_p values are varied. The small-signal model was linearized by keeping the PLL dynamics and SCR of the grid into account to develop a transfer function. This transfer function is used to derive the pole map that displays the stability of the system.

As K_p gain decreased from 180 to 1, poles began to migrate more to the right-hand plane (RHP), which depicted the system as unstable. K_p gain being 1 is the lowest gain showing the worst-case scenario the grid can be, which is classified as unstable. At this point, the pole has fully migrated to the right-hand plane.

CHAPTER 5

CONCLUSION

This chapter concludes with a summary of the work done. It provides suggestions to what could be done to enhance the study discussed in this work. It also provides potential work that is currently under consideration.

5.1 Summary of Present Work

A DG interconnected grid system was discussed in this work by first outlining its benefits to increasing power generation, reducing carbon emission, and it's readily available for consumption. Power electronic technology makes it possible for the efficient use of this energy from where it is produced to where it is consumed. The technology comes with its sets of problems as demand increases, and so does the system complexity. One of these problems is its introduction of instability to the grid.

One of the technologies that has made it possible for the integration of renewable energy is the VSC. It allows the conversion of power from dc to ac and can also do the reverse depending on the application. Various factors contributing to grid instability were enumerated in this work, but the focus was on the effect of the PLL dynamics on the grid. The PLL allows the VSC converter to sync with the grid frequency and maintain stability. The effect of the PLL dynamics on the grid impedance was observed, and its negative effect on the grid was presented. A solution to this problem could be to re-tune the PLL filter dynamics during weak-grid conditions to improve the ac-bus voltage dynamics, but this is not pragmatic as it may limit performance. The pole map, together with the real and reactive power control stability, was simulated to display the state of the stability of the system. It was demonstrated that once the SCR$<$2, the system stability is more susceptible to changes by the K_p gains.

A strong relationship could be seen between the grid impedance and SCR. As the

inductance of the ac-bus voltage dynamics increases, an inverse effect can be noted on the grid stiffness. The PLL was seen to have no effect under a very stiff grid, but under the weak-grid condition, coupling between the converter and grid dynamic increases, so does the dependence on the ac-bus voltage.

At a very strong grid condition, there was no effect on grid stability at various PLL gain K_p. The system maintained stability even when reduced to the lowest K_p gain of 1. At weak-grid conditions, the system is more stable when the PLL gain is set to the optimal gain value, and this parameter variation depends on the capacitor and inductor VSC output filter values.

5.2 Future Work

A robust simulation taking into account other factors that were not considered in the Thévenin equivalent model would provide a better insight into the threshold of the PLL gain that would increase efficiency and stability.

Other external factors, such as faults, can be analyzed to demonstrate the PLL's dynamic effect on the grid strength and how it handles system stability during such conditions.

There are some problems that mathematical models and simulations do not take into account, that are issues in the real world. Further studies can explore the relationship between the grid strength and the PLL by providing an insight through experiments in the lab.

As the grid changes from a strong grid (SCR=10) to a weak grid (SCR$<$3), the system becomes more unstable. This instability leads to grid frequency instability, inadequate active power, and reactive power control.

REFERENCES

[1] A. A. A. Radwan and Y. A. I. Mohamed, "Linear active stabilization of converter-dominated DC microgrids," *IEEE Transactions on Smart Grid*, vol. 3, no. 1, pp. 203–216, 2012.

[2] A. Kwasinski and C. N. Onwuchekwa, "Dynamic behavior and stabilization of DC microgrids with instantaneous constant- power loads," *IEEE Transactions on Power Electronics*, vol. 26, no. 3, pp. 822–834, 2011.

[3] A. Kwasinski, "Quantitative evaluation of DC microgrids availability: Effects of system architecture and converter topology design choices," *IEEE Transactions on Power Electronics*, vol. 26, no. 3, pp. 835–851, 2011.

[4] R. S. Balog, W. W. Weaver, and P. T. Krein, "The load as an energy asset in a distributed DC smartgrid architecture," *IEEE Transactions on Smart Grid*, vol. 3, no. 1, pp. 253–260, 2012.

[5] N. Hatziargyriou, H. Asano, R. Iravani, and C. Marnay, "Microgrids," *IEEE Power and Energy Magazine*, vol. 5, no. 4, pp. 78– 94, 2007.

[6] X. Liu, P. Wang, and P. C. Loh, "A hybrid AC/DC microgrid and its coordination control," *IEEE Transactions on Smart Grid*, vol. 2, no. 2, pp. 278–286, 2011.

[7] A. A. A. Radwan and Y. A. I. Mohamed, "Assessment and mitigation of interaction dynamics in hybrid AC/DC distribution generation systems," *IEEE Transactions on Smart Grid*, vol. 3, no. 3, pp. 1382–1393, 2012.

[8] D. Chen and L. Xu, "Autonomous DC voltage control of a DC microgrid with multiple slack terminals," *IEEE Transactions on Power Systems*, vol. 27, no. 4, pp. 1897–1905, 2012.

[9] M. Davari and Y. A. I. Mohamed, "Robust multi-objective control of VSC-based DC-voltage power port in hybrid AC/DC multi-terminal micro-grids," *IEEE Transactions on Smart Grid*, vol. 4, no. 3, pp. 1597–1612, 2013.

[10] H. Kakigano, Y. Miura, T. Ise, and R. Uchida, "DC voltage control of the DC microgrid for super high quality distribution," in *2007 Power Conversion Conference - Nagoya*, 2007, pp. 518–525.

[11] J. Lee, B. Han, and N. Choi, "DC micro-grid operational analysis with detailed simulation model for distributed generation," in *2010 IEEE Energy Conversion Congress and Exposition*, 2010, pp. 3153–3160.

[12] D. Kumar, F. Zare, and A. Ghosh, "DC microgrid technology: System architectures, AC grid interfaces, grounding schemes, power quality, communication networks, applications, and standardizations aspects," *IEEE Access*, vol. 5, pp. 12 230–12 256, 2017.

[13] M. Saeedifard, M. Graovac, R. F. Dias, and R. Iravani, "DC power systems: Challenges and opportunities," in *IEEE PES General Meeting*, 2010, pp. 1–7.

[14] M. Davari and Y. A. I. Mohamed, "Dynamics and robust control of a grid-connected VSC in multiterminal DC grids considering the instantaneous power of DC- and AC-side filters and DC grid uncertainty," *IEEE Transactions on Power Electronics*, vol. 31, no. 3, pp. 1942–1958, 2016.

[15] C. Chu and H. H. Iu, "Complex networks theory for modern smart grid applications: A survey," *IEEE Journal on Emerging and Selected Topics in Circuits and Systems*, vol. 7, no. 2, pp. 177–191, 2017.

[16] M. Barnes, D. Van Hertem, S. P. Teeuwsen, and M. Callavik, "HVDC systems in smart grids," *Proceedings of the IEEE*, vol. 105, no. 11, pp. 2082–2098, 2017.

[17] D. S. Miranda, Y. Sun, J. F. G. Cobben, and M. Gibescu, "Impact of energy storage on island grid dynamics: A case study of bonaire," in *2016 IEEE International Energy Conference (ENERGYCON)*, 2016, pp. 1–7.

[18] S. A. Khajehoddin, M. Karimi-Ghartemani, and M. Ebrahimi, "Grid-supporting inverters with improved dynamics," *IEEE Transactions on Industrial Electronics*, vol. 66, no. 5, pp. 3655–3667, 2019.

[19] J. Fang, P. Lin, H. Li, Y. Yang, and Y. Tang, "An improved virtual inertia control for three-phase voltage source converters connected to a weak grid," *IEEE Transactions on Power Electronics*, vol. 34, no. 9, pp. 8660– 8670, 2019.

[20] M. Davari and Y. A. I. Mohamed, "Variable-structure-based nonlinear control for the master VSC in DC-energy-pool multiterminal grids," *IEEE Transactions on Power Electronics*, vol. 29, no. 11, pp. 6196–6213, 2014.

[21] M. Boyra and J. Thomas, "A review on synchronization methods for grid-connected three-phase VSC under unbalanced and distorted conditions," in *Proceedings of the 2011 14th European Conference on Power Electronics and Applications*, 2011, pp. 1–10.

[22] M. Karimi-Ghartemani and M. R. Iravani, "A method for synchronization of power electronic converters in polluted and variable-frequency environments," *IEEE Transactions on Power Systems*, vol. 19, no. 3, pp. 1263–1270, 2004.

[23] M. Shamim Reza and V. G. Agelidis, "A demodulation-based technique for robust estimation of single-phase grid voltage fundamental parameters," *IEEE Transactions on Industrial Informatics*, vol. 13, no. 1, pp. 166–175, 2017.

[24] S. Golestan, A. Vidal, A. G. Yepes, J. M. Guerrero, J. C. Vasquez, and J. Doval-Gandoy, "A true open-loop synchronization technique," *IEEE Transactions on Industrial Informatics*, vol. 12, no. 3, pp. 1093–1103, 2016.

[25] A. Jos, *High Voltage Direct Current Transmission*, 2nd ed. Institution of Electrical Engineers, 1998, ch. 1, pp. 1–9.

[26] L. Zhang, L. Harnefors, and H. Nee, "Power-synchronization control of grid-connected voltage-source converters," *IEEE Transactions on Power Systems*, vol. 25, no. 2, pp. 809–820, 2010.

[27] O. B. Nayak, A. M. Gole, D. G. Chapman, and J. B. Davies, "Dynamic performance of static and synchronous compensators at an HVDC inverter bus in a very weak AC system," *IEEE Transactions on Power Systems*, vol. 9, no. 3, pp. 1350–1358, 1994.

[28] A. Yazdani and R. Iravan, *Voltage-Sourced Converters In Power Systems*. John Wiley and Sons, Inc., 2010, ch. 4.

[29] Jih-Sheng Lai and Fang Zheng Peng, "Multilevel converters-a new breed of power converters," *IEEE Transactions on Industry Applications*, vol. 32, no. 3, pp. 509–517, 1996.

[30] J. Rodriguez, J. Pontt, G. Alzarnora, N. Becker, O. Einenkel, and A. Weinstein, "Novel 20-mw downhill conveyor system using three-level converters," *IEEE Transactions on Industrial Electronics*, vol. 49, no. 5, pp. 1093–1100, 2002.

[31] J. Rodriguez, Jih-Sheng Lai, and Fang Zheng Peng, "Multilevel inverters: a survey of topologies, controls, and applications," *IEEE Transactions on Industrial Electronics*, vol. 49, no. 4, pp. 724–738, 2002.

[32] S. S. Baghsorkhi and I. A. Hiskens, "Analysis tools for assessing the impact of wind power on weak grids," in *2012 IEEE International Systems Conference SysCon 2012*, 2012, pp. 1–8.

[33] X. I. Koutiva, T. D. Vrionis, N. A. Vovos, and G. B. Giannakopoulos, "Optimal integration of an offshore wind farm to a weak AC grid," *IEEE Transactions on Power Delivery*, vol. 21, no. 2, pp. 987–994, 2006.

[34] "IEEE guide for planning DC links terminating at AC locations having low short-circuit capacities," *IEEE Std 1204-1997*, pp. 1–216, 1997.

[35] C. K. J. A. Fitzgerald and S. D. Umans, *Electric Machinery*, 6th ed. McGraw-Hill, 2005.

[36] P. Kundur, *Power System Stability and Control. New York:*. McGraw-Hill, 1993.

[37] R. E. Best, *Phase-locked Loops: Theory, Design, and Applications*, 2nd ed. New York: McGraw-Hill, 1993.

[38] V. I. Utkin, "Sliding mode control design principles and applications to electric drives," *IEEE Transactions on Industrial Electronics*, vol. 40, no. 1, pp. 23–36, 1993.

[39] T. Noguchi, H. Tomiki, S. Kondo, and I. Takahashi, "Direct power control of PWM converter without power-source voltage sensors," *IEEE Transactions on Industry Applications*, vol. 34, no. 3, pp. 473–479, 1998.

[40] C. Schauder and H. Mehta, "Vector analysis and control of advanced static var compensators," *IEE Proceedings C - Generation, Transmission and Distribution*, vol. 140, no. 4, pp. 299–306, 1993.

[41] P. Mattavelli, L. Rossetto, G. Spiazzi, and P. Tenti, "General-purpose sliding-mode controller for DC/DC converter applications," in *Proceedings of IEEE Power Electronics Specialist Conference - PESC '93*, 1993, pp. 609–615.

[42] K. Jezernik and D. Zadravec, "Sliding mode controller for a single phase inverter," in *Fifth Annual Proceedings on Applied Power Electronics Conference and Exposition*, 1990, pp. 185–190.

[43] R. O. Caceres and I. Barbi, "A boost DC-AC converter: analysis, design, and experimentation," *IEEE Transactions on Power Electronics*, vol. 14, no. 1, pp. 134–141, 1999.

[44] M. Malinowski, M. Jasinski, and M. P. Kazmierkowski, "Simple direct power control of three-phase PWM rectifier using space-vector modulation (DPC-SVM)," *IEEE Transactions on Industrial Electronics*, vol. 51, no. 2, pp. 447–454, 2004.

[45] M. Malinowski, M. P. Kazmierkowski, S. Hansen, F. Blaabjerg, and G. D. Marques, "Virtual-flux-based direct power control of three-phase PWM rectifiers," *IEEE Transactions on Industry Applications*, vol. 37, no. 4, pp. 1019–1027, 2001.

[46] L. Xu, D. Zhi, and L. Yao, "Direct power control of grid connected voltage source converters," in *2007 IEEE Power Engineering Society General Meeting*, 2007, pp. 1–6.

[47] R. Datta and V. T. Ranganathan, "Direct power control of grid-connected wound rotor induction machine without rotor position sensors," *IEEE Transactions on Power Electronics*, vol. 16, no. 3, pp. 390–399, 2001.

[48] M. Davari and Y. A. I. Mohamed, "Robust vector control of a very weak-grid-connected voltage-source converter considering the phase-locked loop dynamics," *IEEE Transactions on Power Electronics*, vol. 32, no. 2, pp. 977–994, 2017.

[49] L. Zhang, L. Harnefors, and P. Mitra, "Offshore wind integration to a weak grid by VSC-HVDC links using power-synchronization control: A case study," in *2014 IEEE PES General Meeting — Conference Exposition*, 2014, pp. 1–1.

[50] L. Harnefors, M. Bongiorno, and S. Lundberg, "Input-admittance calculation and shaping for controlled voltage-source converters," *IEEE Transactions on Industrial Electronics*, vol. 54, no. 6, pp. 3323–3334, 2007.

[51] M. Durrant, H. Werner, and K. Abbott, "Model of a VSC HVDC terminal attached to a weak AC system," in *Proceedings of 2003 IEEE Conference on Control Applications, 2003. CCA 2003.*, vol. 1, 2003, pp. 178–182 vol.1.

[52] A. Egea-Alvarez, S. Fekriasl, and O. Gomis-Bellmunt, "Advanced vector control for voltage source converters connected to weak grids," in *2016 IEEE Power and Energy Society General Meeting (PESGM)*, 2016, pp. 1–1.

[53] M. P. Kazmierkowski and L. Malesani, "Current control techniques for three-phase voltage-source PWM converters: a survey," *IEEE Transactions on Industrial Electronics*, vol. 45, no. 5, pp. 691–703, 1998.

[54] J. Z. Zhou, H. Ding, S. Fan, Y. Zhang, and A. M. Gole, "Impact of short-circuit ratio and phase-locked-loop parameters on the small-signal behavior of a VSC-HVDC converter," *IEEE Transactions on Power Delivery*, vol. 29, no. 5, pp. 2287–2296, 2014.